



**EUROfusion**

WPEDU-PR(18) 20986

L Ballauf et al.

**Tritium retention: Synthesis of beryllium hydrides in chemical sputtering by deuterium from 20 to 420 eV**

Preprint of Paper to be submitted for publication in  
Nuclear Fusion



This work has been carried out within the framework of the EUROfusion Consortium and has received funding from the Euratom research and training programme 2014-2018 under grant agreement No 633053. The views and opinions expressed herein do not necessarily reflect those of the European Commission.

This document is intended for publication in the open literature. It is made available on the clear understanding that it may not be further circulated and extracts or references may not be published prior to publication of the original when applicable, or without the consent of the Publications Officer, EUROfusion Programme Management Unit, Culham Science Centre, Abingdon, Oxon, OX14 3DB, UK or e-mail [Publications.Officer@euro-fusion.org](mailto:Publications.Officer@euro-fusion.org)

Enquiries about Copyright and reproduction should be addressed to the Publications Officer, EUROfusion Programme Management Unit, Culham Science Centre, Abingdon, Oxon, OX14 3DB, UK or e-mail [Publications.Officer@euro-fusion.org](mailto:Publications.Officer@euro-fusion.org)

The contents of this preprint and all other EUROfusion Preprints, Reports and Conference Papers are available to view online free at <http://www.euro-fusionscipub.org>. This site has full search facilities and e-mail alert options. In the JET specific papers the diagrams contained within the PDFs on this site are hyperlinked

1 *Tritium retention: Synthesis of beryllium*  
2 *hydrides in chemical sputtering by*  
3 *deuterium from 20 to 420 eV*

4 **Authors**

5 Lorenz Ballauf (1)

6 Faro Hechenberger (1)

7 Reinhard Stadlmayr (2)

8 Matthias Daxner (1)

9 Samuel Zöttl (1)

10 Friedrich Aumayr (2)

11 Zdenek Herman (1,3)

12 Paul Scheier (1)

- 13
- 14 1. Institute for Ion Physics and Applied Physics, University of Innsbruck, Technikerstr.  
15 25, 6020 Innsbruck, Austria
- 16 2. Institute of Applied Physics, TU Wien, Fusion@ÖAW, Wiedner Hauptstraße 8-  
17 10/E134, 1040 Vienna, Austria
- 18 3. V. Čermak Laboratory, J. Heyrovský Institute of Physical Chemistry, v.v.i., Academy  
19 of Sciences of the Czech Republic, Dolejškova 3, 18223 Prague 8, Czech Republic

20

# 21 **Keywords**

22 beryllium hydride, tritium retention, low energy sputtering, chemical sputtering, BeD,  
23 thermonuclear fusion, co-deposition

# 24 **Contents**

25	<b>1 Abstract</b>	<b>3</b>
26	<b>2 Introduction</b>	<b>3</b>
27	<b>3 Experimental setup</b>	<b>5</b>
28	<b>4 Experimental procedure</b>	<b>7</b>
29	<b>5 Results and discussion</b>	<b>9</b>
30	<i>5.1 In situ sputter cleaning</i>	<i>10</i>
31	<i>5.2 Formation of BeD<sup>+</sup>: the projectile reaction</i>	<i>10</i>
32	5.2.1 Energy scan	10
33	5.2.2 Temperature scan	13
34	5.2.3 Projectile current scan	14
35	<i>5.3 Formation of BeH<sup>+</sup>: the surface adsorbate channel</i>	<i>16</i>
36	5.3.1 C <sub>6</sub> H <sub>14</sub> pressure scan	16
37	5.3.2 H <sub>2</sub> O pressure scan	17
38	<i>5.4 TOF-ERDA: elemental composition profile</i>	<i>18</i>
39	<b>6 Conclusion and outlook</b>	<b>20</b>
40	<b>7 Acknowledgments</b>	<b>21</b>
41	<b>8 References</b>	<b>21</b>
42	<b>9 Supplementary material</b>	<b>24</b>
43	9.1.1 D <sub>2</sub> pressure scan, D <sub>2</sub> <sup>+</sup> projectile	24
44	9.1.2 D <sub>2</sub> pressure scan, He <sup>+</sup> projectile	25
45	9.2 Temperature scan, relative yield	26
46	9.3 Current scan, absolute yield	26
47	9.4 3D surface profile	27
48		

# 49 1 Abstract

50 This work describes the formation of beryllium hydrides in collisions of deuterium ions with a  
51 beryllium surface. These chemical sputtering products have been experimentally resolved by  
52 mass spectrometry. In the manifold of products, beryllium hydride is of special interest as a  
53 candidate for tritium retention in thermonuclear fusion devices. Our experiments show, that it  
54 can be synthesized in nearly all conditions comparable to plasma and wall temperature, with  
55 two mechanisms involved: First,  $\text{BeD}^+$  is formed directly in a reaction of the  $\text{D}_2^+$  molecules  
56 with the bulk beryllium surface, which is the main aspect of this work. Focusing on  $\text{Be}^+$ ,  
57  $\text{BeH}^+$  and  $\text{BeD}^+$  products, their dependence on different parameters is measured: Scanning the  
58 impact energy from 20 to 426 eV reveals that the molecular  $\text{BeD}^+$  is preferably produced at  
59 low energies. Surprisingly its yield is three times higher than that of pure  $\text{Be}^+$  at 20 eV. When  
60 the surface temperature is raises from 298 to 673 K, sputtering yields increase two orders of  
61 magnitude for both,  $\text{Be}^+$  and  $\text{BeD}^+$ . The second reaction pathway produces  $\text{BeH}^+$ . It is  
62 efficiently synthesized from water vapor adsorbed on the surface, much less abundant from  
63 hexane and hydrogen adsorbates. In general, such surface experiments are very challenging  
64 and great care has been taken to rule out experimental concerns systematically, using the  
65 measurements above in combination with an element composition profile of the beryllium  
66 sample.

# 67 2 Introduction

68 Hydrogen and its isotopes can be trapped in bulk material. In the context of fusion devices  
69 like ITER, JET or many more, this is commonly called “tritium retention”. The radioactivity  
70 of tritium then poses a security threat, as in an accident this tritium might be released into the  
71 environment. As an example, for ITER, the maximum tritium inventory may not exceed 0.7  
72 kg [1]. Therefore, operating intervals between cleaning interruptions are limited. Estimates  
73 are between two months [2] and only one week [3], they still have “extremely large  
74 uncertainties” [2]. In this sense tritium retention could make thermonuclear fusion unfeasible  
75 in a commercial implementation.

76 There is strong evidence that most of the tritium is retained in the divertor region of fusion  
77 devices [1], [2], [4]. Above the bulk tungsten, a thin film (e.g. 40  $\mu\text{m}$  in JET ILW [1]) of co-  
78 deposition between tritium and beryllium was found. So the beryllium starts in the upper parts

79 of the vessel (PFC in the blanket), in a region of net-erosion by the plasma wall interaction  
80 and forms some sort of compound with tritium as it migrates towards the divertor. This  
81 happens in a series of deposition and re-emission cycles, until it finally ends up in the vacuum  
82 pumping system, or in a “cold” region of net-growth in the divertor. It is not clear, where this  
83 compound is formed (gas phase / surface), nor, if it is a rather physical or chemical process.

84 Our measurements show, that, at least partly, this compound consists of molecules, directly  
85 formed in the sputter process on the surface. We cannot provide a quantitative analysis of  
86 their relevance for fusion devices. This is the domain of tailored simulations that make use of  
87 our data. Experimentally, we find  $\text{BeD}^+$  and  $\text{BeH}^+$ , pointing towards charged and neutral BeT.  
88 Indeed, BeD was found in the co-deposition layer in question [5] in the PISCES-B experiment  
89 [6]. There, the source of the BeD molecules remains quite unclear and is argued to be a gas-  
90 phase reaction. By assuming a much lower kinetic energy of BeD relative to the surface in  
91 comparison with Be, their intensity profiles at a given target distance should be different  
92 when BeD is produced on the surface [7], but this is not the case. At least for the ionic  
93 fraction, however, we have measured that the kinetic energy of  $\text{BeD}^+$  and  $\text{Be}^+$  is the same (at a  
94 given projectile energy), simply by varying the surface potential. Thus, the gas phase  
95 justification described above does not hold for at least the ionic fraction. Additionally, an ion-  
96 surface interaction is conceptually more likely for the pressures present in fusion devices.

97 At first glance, molecule formation seems not to be important for a plasma device, as any  
98 molecule that is emitted deep into the plasma will immediately fragment. But the same is true  
99 for any process that could create the co-deposited material in question, so today molecules are  
100 seen as a substantial challenge for plasma wall interactions [8]. Additionally, the charged  
101 species discussed here will follow the magnetic field lines towards the divertor, being guided  
102 away from the hot core, in contrast to neutrals. For a stable chemical species, the relevant re-  
103 emission cycles are obviously those where the particle energy or plasma temperature is low.  
104 We show below that the relative yield for  $\text{BeD}^+$  is strongly increasing with lowering the  
105 projectile energy, which would lead to a hydride-enrichment during the re-emission cycles. It  
106 is not just this qualitative fit to the analysis from JET ILW surface samples that makes our  
107 approach valuable. Data on molecules have been requested [2], but there are only few  
108 experiments that can access the low-energy sputtering regime [9]–[11]. These studies on the  
109 beryllium-deuterium ion surface system often suggest the low-energy sputtering threshold  
110 energy to be lower than expected from fitting the Bohdansky formula, due to a lowering of  
111 the Be surface binding energy by surface roughness [9]. However, they usually lack the  
112 chemical analysis in situ and suffer from larger errors [9]. Our studies show that these results

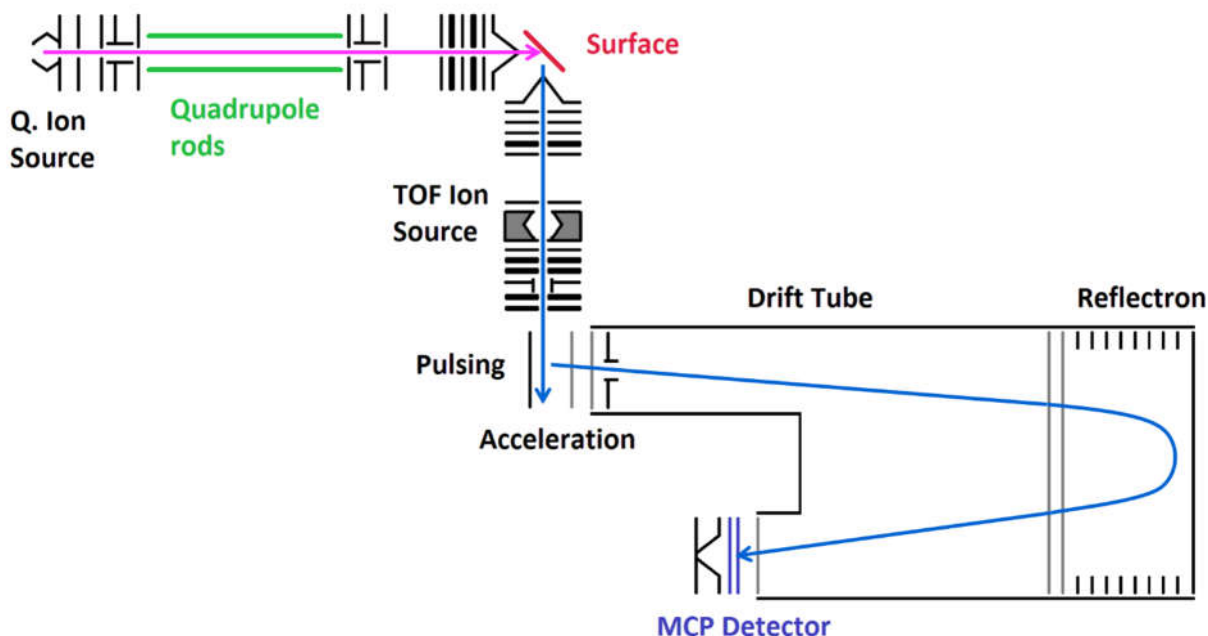
113 may be altered by the increased  $\text{BeD}^+$  chemical sputtering yield not being distinguished from  
114 the pure Be yield.

115 To our knowledge, there are currently no experimental setups that can analyze the chemical  
116 composition of sputter products in situ providing good data quality, sensitivity and  
117 permanently clean surface conditions. Conceptually similar experiments suffered from surface  
118 hydrocarbon films on top of the surface [12]–[18], generated by pump oil adsorption (also  
119 with turbopumps). The newly constructed apparatus (SurfTOF, Surface Time-of-Flight),  
120 achieves a hydrocarbon free surface by in situ sputter cleaning via a high projectile ion flux.  
121 Besides causing repeatable measurements, this also opens the way to proper measurements of  
122 how neutral molecules, intentionally adsorbed to the surface, influence sputter products. As a  
123 simple example, water will adsorb much less on a surface if there are hydrocarbons present  
124 [19]. This work includes first data on adsorption as well. With only minor relevance to fusion  
125 devices (reactions of cooling water impurities in a tokamak), the purpose here is to understand  
126 and evaluate the ion beam method itself more deeply.

127 Pressures are mutually comparable to SurfTOF (ITER:  $10^{-8}$  mbar background [20], up to 0,1  
128 mbar in the neutral pumping section [21]). Other experimental conditions, like surface  
129 temperature and particle energy can be adjusted to resemble different parts of a fusion device.  
130 The surface ion flux of particles per area and per time is much lower in an ion beam device.  
131 However, measurements with variable flux could be performed for the first time, indicating  
132 whether a certain process discovered depends on the flux or not.

### 133 **3 Experimental setup**

134 The idea of this experiment is an MS-MS technique or tandem mass spectrometer with a  
135 surface placed between the two mass spectrometers.



136  
137

138 *1: Sketch of the SurfTOF experiment. Arrows indicate the ion flightpath, Electrostatic lenses*  
 139 *drawn schematically. The vacuum system encloses the whole experiment, with differential*  
 140 *pumping across the quadrupole, in order to maintain a low pressure in the chamber*  
 141 *containing the surface.*

142 Projectile ions are generated in an electron ionization source, with the ionization potential  
 143 kept at 100 V, except for the He<sup>+</sup> measurements it is raised to 200 V. Ions are then focused  
 144 into a quadrupole mass filter. This “m/z selected ion gun” is a highly modified Pfeiffer QMA  
 145 400 quadrupole, delivering up to 80 nA ion current to the surface, depending on the projectile  
 146 and resolution settings. The mean impact energy results from the potential difference between  
 147 the ionization region and the surface itself (between 5 and 500 V) which gives good energy  
 148 resolution (smaller than 1 eV) for the projectiles used in this study.

149 The impact and analysis is kept at 45° to the surface. This collision region is field-free, only  
 150 the charged sputtering products that make it past the conical lens can be transported towards  
 151 the analysis section of the experiment. The filaments of the TOF ion source are usually  
 152 switched off, only its lenses are used to focus product ions into the acceleration region of the  
 153 home built, orthogonal pulsing, reflectron time-of-flight (TOF) mass spectrometer.

154 Although this looks similar to a SIMS (secondary ion mass spectrometer), it is entirely  
 155 different. The aim utilizing SurfTOF is to observe chemical reactions and low energy  
 156 sputtering behavior, whereas SIMS analyzes the surface content trying not to trigger  
 157 reactions. Hence, the projectile energy differs by several orders of magnitude. Moreover, the



158 surface region is not field free in a SIMS experiment and the equilibrium conditions described  
159 in the experimental procedure are not met.

160 The instrument can also be used as a high precision residual gas analyzer. By switching on the  
161 TOF ion source, the residual gas in the surface vacuum chamber can be monitored, handy for  
162 impurity-sensitive surface experiments. Additional checks are possible: When a repulsive  
163 potential is applied to the surface, one can bend the ion beam towards the TOF, without a  
164 surface collision. This allows monitoring the quadrupole mass selection and therefore the  
165 purity of the projectile beam. Furthermore, the residual gas in the quadrupole ion source can  
166 be analyzed, when the quadrupole is switched to the ion guide mode.

167 The surface can be heated, up to 730 K, the temperature is measured by a Type-K  
168 thermocouple. The surface current is measured with a pA-meter (rbd instruments 9103).

169 The vacuum is generated by turbomolecular pumps (Pfeiffer) that are oil-free on the high  
170 vacuum side. The base pressure is  $1.5 \times 10^{-8}$  mbar, which is sufficient as shown later. The  
171 neutral gas can be introduced in a very controlled way: in collaboration with  
172 pressurecontrolsolutions.nl a PID controller was developed, that uses the analog signal from  
173 the cold cathode vacuum gauges to control a proportional valve. This ensures stable pressures  
174 (relative standard deviation typically 0.003) and ion currents. Additionally, it is designed to be  
175 leak tight and allows to start and stop gas flow safely via the measurement PC. A gas barrier  
176 allows for differential pumping of the quadrupole ion source and surface chamber, creating  
177 pressure differences of up to two orders of magnitude.

## 178 **4 Experimental procedure**

179 Surface experiments in general, low-energy ones especially, are difficult with respect to  
180 repeatability and stability. The new experiment allows us to monitor and reach, what we call  
181 equilibrium condition. The idea is the following: The peaks in mass-spectra obtained from a  
182 surface, may not be constant over time, if the underlying processes are slow. As an example,  
183 if the sputter yield of a certain product relies on projectile implantation and re-emission by  
184 projectiles coming later, it will increase over time until it reaches a steady state. Those are  
185 rather slow processes and influence the yields measured over hours or even days. There are  
186 two ways to monitor, if the investigated process has reached its equilibrium. First, the  
187 intensity of many peaks is high enough to trace temporal behavior and thus stability. For  
188 peaks close to the detection limit, the equilibrium conditions are checked in the following

189 way: Usually, one parameter (e.g. projectile energy), is scanned between single mass spectra  
190 taken. Such a scan is not performed one-after the other (e.g. 20, 30, 40 eV...), but in a random  
191 order (e.g. 30, 320, 50 eV...). Later the plot of the scan (e.g. figure 4) is checked for extensive  
192 scatter. If this was not done, one cannot attribute a change in yield to a parameter change. It  
193 might simply be a slow diffusion, whose variation in time would be interpreted wrongly as a  
194 dependence on the parameter investigated. Only if these checks are passed, we refer to a  
195 process as having reached equilibrium conditions. Thereby, results are reproducible, even if  
196 the measurements are months apart or the sample was exposed to the atmosphere. We  
197 attribute this exceptional stability also to the high surface currents in general.

198 Scatter in random parameter scans is also the best estimate for systematic error. As can be  
199 seen from the data (figure 3 to 8), it is very low for most products. Statistical errors are: The  
200 counting error, slight instabilities of the surface temperature (max. +/- 4 K), the pressure error,  
201 estimated as the standard deviation of all the samples in one measurement. The correction  
202 factor for each gas measured in the cold cathode gauges is obtained from the electron  
203 ionization cross section at 100 eV [22].

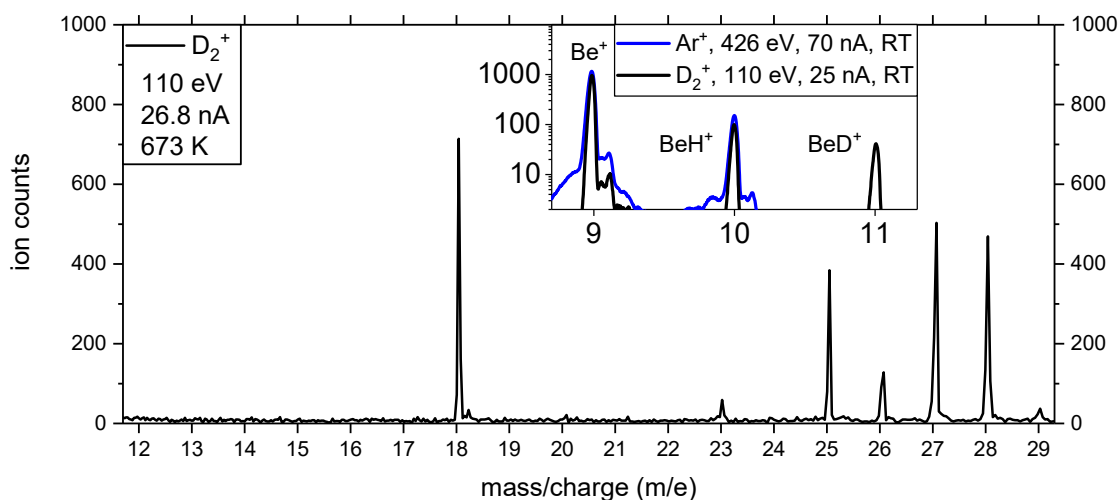
204 The surface current is sampled before and after a measurement and their difference is denoted  
205 as the error bar. The error of the impact energy is smaller than the symbols in the graphs.  
206 Straight lines between single measurement points are drawn as a guide to the eye, having no  
207 physical meaning.

208 Data analysis is straightforward, as a mass-peak of interest is summed up in the raw TOF data  
209 and a constant background correction subtracted, estimated from signal free parts in the  
210 spectra. This noise is low, for example 0.3 % of the  $\text{BeD}^+$  peak area in figure 2. Throughout  
211 this work, absolute yield refers to this number of ions divided by the number of TOF scans  
212 and divided by the surface current in Ampere, leading to units of  $\frac{\text{ion counts}}{N_{\text{scans}} \times A} = \text{A}^{-1}$ . The  
213 normalization factor ( $N_{\text{scans}} \times I_{\text{surf}}$ ) is around 10 for an overnight and typically 1 for a two-  
214 hour measurement. The so-called relative yield is obtained, when the number of ions in the  
215 peak of interest is divided by the number of  $\text{Be}^+$  ions in that measurement. This efficiently  
216 cancels many instabilities, being small they influence the  $\text{Be}^+$  yield linearly, so the latter  
217 becomes an in situ probe for instabilities. Additionally, the relative yield is essentially an ion  
218 yield ratio, for example the  $\text{BeD}^+/\text{Be}^+$  yield. This can be compared well to other results from  
219 the literature and theory.

220 Preliminary results were compared among different bulk beryllium samples, with little  
221 differences between them. All data shown in this publication was obtained using the same

222 rolled amorphous beryllium sample (obtained from alfa aesar), in order to lower the number  
 223 of possible error sources in mutual comparisons.

## 224 5 Results and discussion



225  
 226 *2: Examples of mass spectra obtained. m/e 9 is Be<sup>+</sup>, m/e 10 is BeH<sup>+</sup>, m/e 11 is BeD<sup>+</sup>, only*  
 227 *produced when using D-containing projectiles (other products discussed in the text). There is*  
 228 *a peak shape issue with ghost peaks on the right of the parent, caused by faulty beam*  
 229 *focusing, but it does not alter analysis, as it repeats on every peak.*

230 We can attribute the following mass to charge ratios from figure 2:

- 231 • m/e 9 is Be<sup>+</sup>, m/e 10 is BeH<sup>+</sup>, m/e 11 is BeD<sup>+</sup>, only produced when using D-containing  
 232 projectiles. BeD<sub>2</sub><sup>+</sup> and BeD<sub>3</sub><sup>+</sup> were not observed.
- 233 • Hydrocarbon residues, for example C, ..., CH<sub>3</sub><sup>+</sup>, m/e 12 – 15 are absent.
- 234 • m/e 18 is mostly Be<sub>2</sub><sup>+</sup>, with only little H<sub>2</sub>O<sup>+</sup> contribution as the OH<sup>+</sup> fragment is  
 235 missing, which was observed when water adsorbed to the surface on purpose  
 236 (H<sub>2</sub>O<sup>+</sup>/OH<sup>+</sup> ≈ 3).
- 237 • m/e 23 is Na<sup>+</sup>, an impurity that has a low neutral content, but its charged yield is large  
 238 due to a high (surface) ionization probability [23].
- 239 • m/e 25 is BeO<sup>+</sup>, m/e 26 is BeOH<sup>+</sup>, m/e 34 (not shown) is abundant as well, associated  
 240 with Be<sub>2</sub>O<sup>+</sup>.

- 241 •  $m/e$  27 could be  $\text{Be}_3^+$ , but  $\text{Be}_4^+$  was not observed.
- 242 •  $m/e$  28 is  $\text{Si}^+$  (compare figure 9), an impurity in the sample, originating from the ore.
- 243  $\text{N}_2^+$  is not expected, the  $\text{N}^+$  fragment is missing.

## 244 **5.1 In situ sputter cleaning**

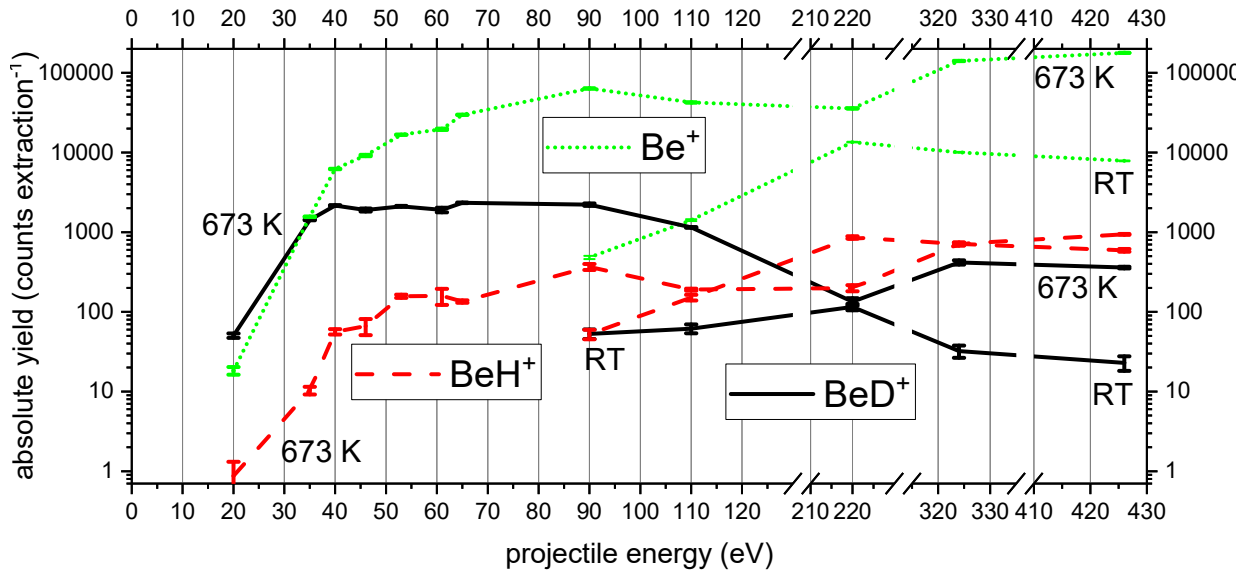
245 As can be seen, the typical mass peaks resulting from hydrocarbon impurities ( $\text{C}$ ,  $\text{CH}^+$ , ...,  
246  $\text{CH}_3^+$  compare figure 2) obtained in similar experiments [24], [25] are completely absent for  
247 the first time. This is achieved via in situ sputter cleaning, simply by the very intense  
248 projectile ions flux. Typically, those products are very intense when a measurement is started,  
249 and decrease over a few hours into a steady state [26]. Its value is determined by the incoming  
250 rate from the background gas, versus the sputter cleaning rate. As the SurfTOF experiment  
251 has a higher projectile flux by 2 to 4 orders of magnitude, the steady state value of  
252 hydrocarbon products is below the detection limit. Consistently, hydrocarbon peaks can only  
253 be seen for a few minutes when a new sample has been put into the setup. To our knowledge,  
254 there is no comparable experiment that has reached this in situ cleaning regime yet.

## 255 **5.2 Formation of $\text{BeD}^+$ : the projectile reaction**

### 256 **5.2.1 Energy scan**

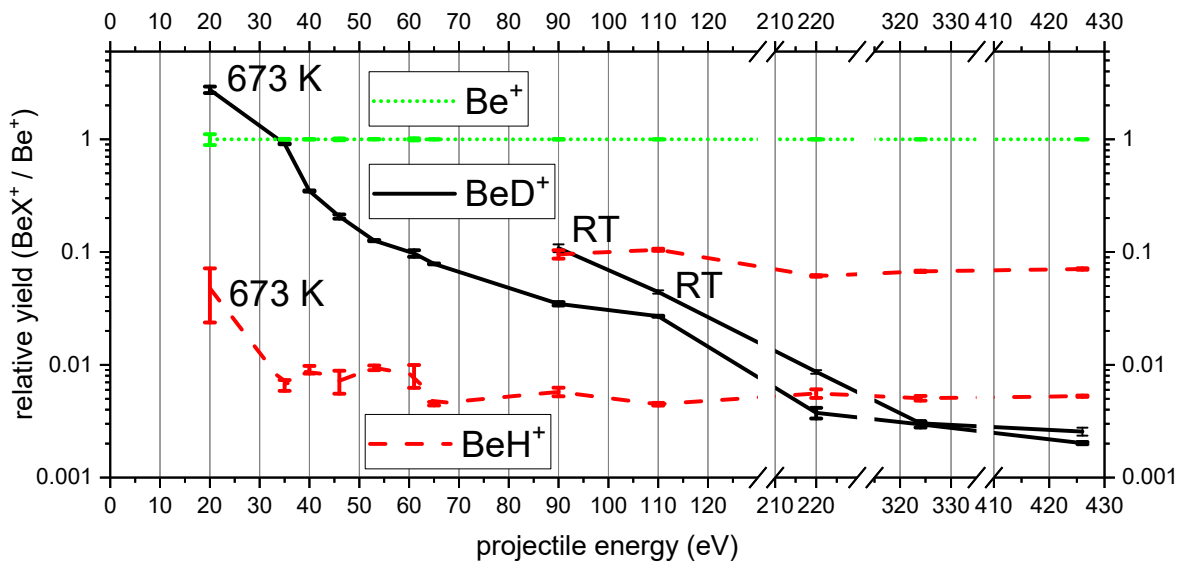
257 The product ion  $\text{BeD}^+$  is formed in a surface reaction between the incident ions  $\text{D}_2^+$  and Be  
258 sample. The absolute yield of  $\text{BeD}^+$  (figure 3) increases from the value at 20 eV to a  
259 maximum at 40 eV and then it decreases at 90 eV and above.  $\text{Be}^+$  increased from the value at  
260 20 eV over the entire energy region. The yield of  $\text{BeH}^+$  followed approximately the yield of  
261  $\text{Be}^+$  at a given  $T_{\text{Surf}}$  and its origin will be discussed later on. The low energy behavior of all  
262 these major product ions indicates a sputtering threshold below 20 eV.

263 The very high relative yield of  $\text{BeD}^+$  (figure 4, 673 K), already above 10 % below 60 eV and  
264 reaching 275 % at only 20 eV, is remarkable. As this curve has no maximum, one may  
265 extrapolate that the relative content of  $\text{BeD}^+$  is the highest at the sputtering threshold.



266  
267

268 *3: Absolute yield for the main products  $Be^+$ ,  $BeH^+$  and  $BeD^+$ . The range covers the transition*  
 269 *from very low energy chemical and potential sputtering to high energy kinetic sputtering.  $T_{Surf}$*   
 270 *is 673 K and 298 K (RT),  $D_2^+$  projectiles. The surface current is 8.0(1) nA for 20 eV, then it*  
 271 *increases from 14.4(2) nA at 35 eV to 23.2(2) nA at 426 eV.*



272

273 *4: Relative yield for the same energy scan. The outstanding feature is that at 20 eV projectile*  
 274 *energy, the  $BeD^+$  yield is nearly 3 times higher than  $Be^+$ .  $BeH^+$  is constant at a given  $T_{Surf}$ ,*  
 275 *except at 20 eV, due to the low 8.0(1) nA  $I_{Surf}$  leading to inefficient sputter cleaning of  $H_2O$ .*

276 As stated in the introduction, the quantitative relevance for fusion devices are difficult to  
 277 derive. This experiment serves for the discovery and qualitative understanding of reactions  
 278 taking place on a surface bombarded with ions. Quantitative analysis has to be done later by  
 279 tailored simulation or specific analysis in tokamaks where possible.

280 Thus, the implication towards tokamak experiments is not straightforward. Allover we find  
281 good qualitative agreement with tokamak data, although there,  $D_2^+$  is very rare,  $D^+$  is the main  
282 projectile. But as the different experimental techniques show the same key features, we expect  
283 that  $D^+$  is at least as reactive as  $D_2^+$  in the  $BeD^+$  synthesis. The bare  $D^+$  was not chosen in this  
284 work, as this would have made access to the ultra-low energy sputtering regime impossible,  
285 due to much lower projectile current. Their difference will be examined in our future work.

286 For the energy scan, we like to compare our data to JET experiments [27]. There, the  
287 projectile energy can only be controlled via the ion temperature, if the surface is directly  
288 exposed to the plasma, i.e. as a beryllium limiter tile. Then, the ion temperature is calculated  
289 from the electron temperature, thus it is less well defined. Also the limited control of  
290 projectile species in a tokamak overlays the beryllium hydride chemical sputtering with Be  
291 self-sputtering above 150 eV. In JET, the neutral  $BeD/Be$  ratio is measured as 1/3, determined  
292 at  $\sim 75$  eV impact energy (similar  $T_{Surf}$ ) [27]. On the one hand, this offset between the ratios  
293 might be attributed to the experimental differences: at JET neutral products are analyzed by  
294 spectroscopy, in contrast to charged products analyzed by mass spectrometry. Also, ionization  
295 probabilities in the sputtering process of Be and  $BeD$  might be different, resulting in  
296 quantitative mismatch between neutral and ionized  $BeD/Be$  ratios. Nevertheless, the  
297 qualitative trends between different experimental methods and theory should still be  
298 comparable (see also the temperature scan, figure 5). Hence, ion beam experiments can  
299 extend the parameter range down to the dilute plasma, low-energy conditions where co-  
300 deposits are formed. These regions could not be monitored in the JET experiment [27], but  
301 are responsible for T retention, as they are the regions of net-deposition. This step in the  
302 parameter range is also the step where  $BeD^+$  molecules can become stable, due to their  
303 standard free energy for dissociation being above 2 eV, even at 1000 K, as derived by theory  
304 [28]. With the ratio of  $T_{ion} = 5 \times T_{electron}$  [27], it is sure that these molecules are stable at cold  
305 regions in the divertor of typically  $T_{ion} = 5$  eV as the electron energy is below the dissociation  
306 threshold.

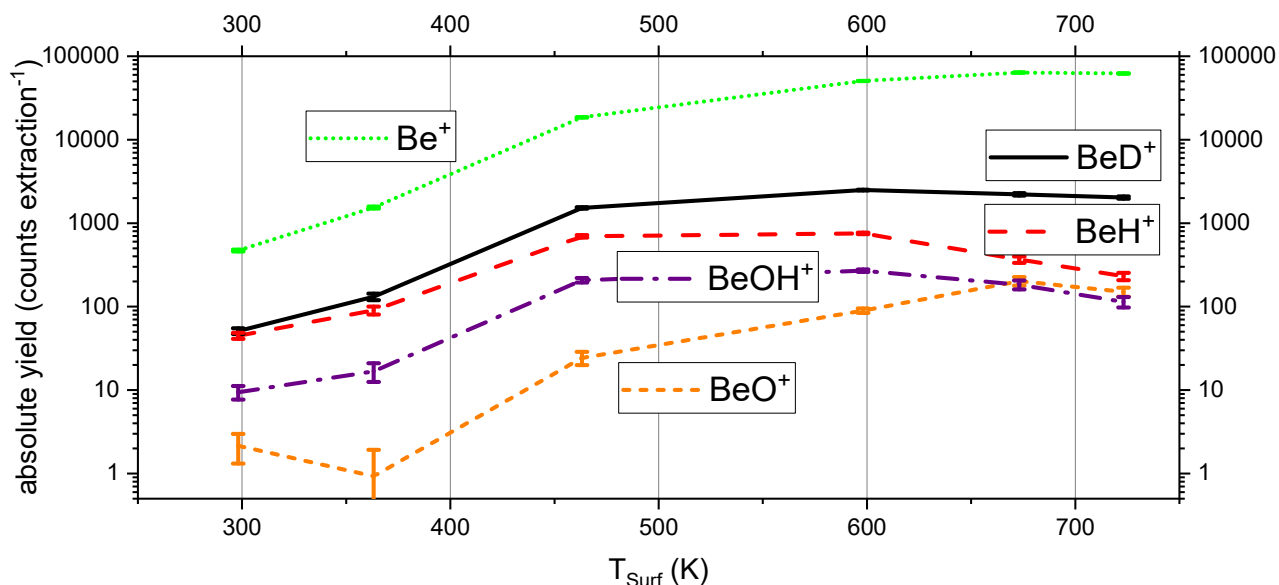
307 The  $BeD^+$  projectile reaction channel may be regarded as equivalent to a  $BeT^+$  channel, which  
308 is one of many potential ways in which tritium can be retained in the reactor wall. The idea of  
309 forming stable molecules, especially at low energies, also agrees well with the experimental  
310 finding, that the removal of T from T-Be co-deposits in tokamaks only by heating might not  
311 be sufficient [1]. It also might offer an answer to the question, why the retention at various  
312 incident particle energies behaves opposite to what is expected from Be co-deposit density  
313 [29], pointing towards the re-emission cycles that enrich hydrides, as discussed in section 1.

314 The high energy part of  $\text{BeD}^+$  dependence in figure 3 and 4 shows a decrease, due presumably  
 315 to the fragmentation of highly internally excited  $\text{BeD}^+$ . However, the absolute yield for  $\text{BeD}^+$   
 316 is still high towards increasing energies, it is also the increasing  $\text{Be}^+$  physical sputtering yield  
 317 that lowers the relative  $\text{BeD}^+$  content – so, even at 426 eV,  $\text{BeD}^+$  is still synthesized on the  
 318 surface.

319 An energy scan was also performed at room temperature (RT, figure 3 and 4). It shows little  
 320 difference in the qualitative behavior, but the absolute yield for  $\text{BeD}^+$  and  $\text{Be}^+$  is substantially  
 321 lower. This behavior was investigated in a temperature scan at fixed impact energy (90 eV,  
 322 figure 5 and 12, supplement).

### 323 5.2.2 Temperature scan

324



325  
326

327 *5: Absolute yields at different  $T_{\text{Surf}}$ . There are two orders of magnitude increase in the  $\text{Be}^+$*   
 328 *yield towards a hot surface, which cannot simply be attributed to  $\text{BeO}$  on the surface.  $\text{BeD}^+$*   
 329 *can be formed on a very hot surface, adsorbate products ( $\text{BeH}^+$ ,  $\text{BeOH}^+$ ) go down.  $\text{D}_2^+$*   
 330 *impacting Be with 90 eV and 16.1(2) nA.*

331 The temperature behavior (figure 5) gives another qualitative match between diverse  
 332 experimental techniques (ion beam, linear plasma and tokamak devices). Not only the  
 333 SurfTOF and JET experiment [27], but also MD simulations [28], [30] find a linear decrease  
 334 of  $\text{BeD}/\text{Be}$  ratio ( $\text{BeD}^+/\text{Be}^+$  respectively, figure 12) with increasing surface temperature. The

335 resulting slopes are comparable within one order of magnitude. This underlines again the  
336 expectation that the more fusion relevant projectile  $D^+$  is at least as reactive as  $D_2^+$ .

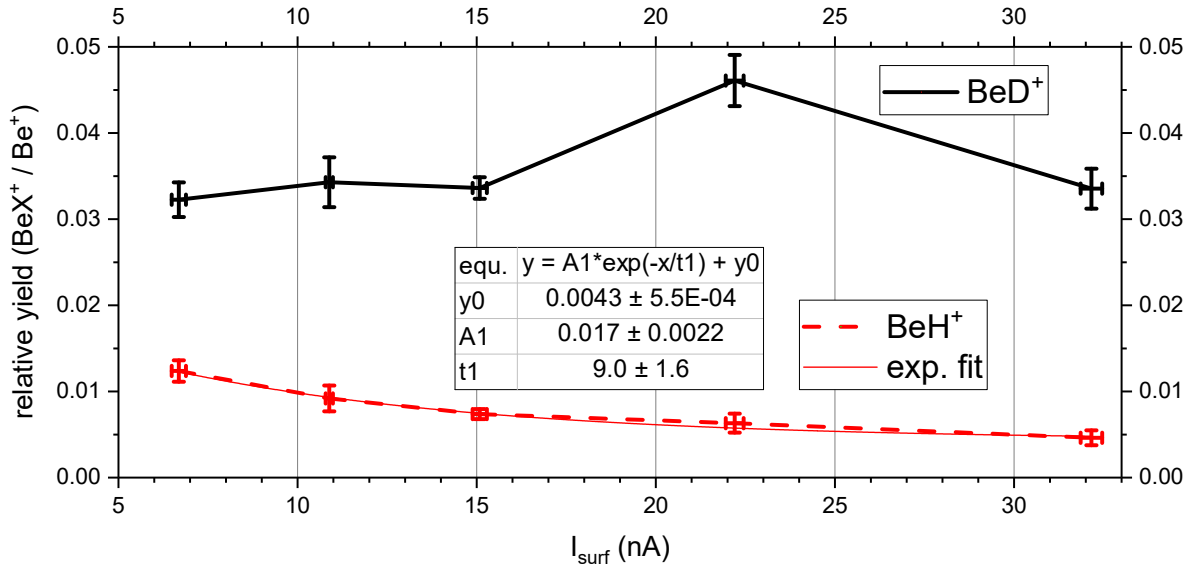
337 There is a pronounced increase in the  $Be^+$  yield for elevated surface temperatures (figure 5).  
338 As we did not observe this for other metals, we doubt that this is only due to the high energy  
339 tail of the thermal distribution approaching the surface binding energy. In the literature, one  
340 finds this attributed to Be starting to diffuse through the oxide layer at higher temperatures,  
341 and BeO has a higher surface binding energy resulting in less sputtering at low temperatures  
342 [10]. If this explanation would also apply to the situation in our experiment, then the  
343  $BeO^+/Be^+$  ratio should drop at elevated temperatures, but it remains constant (rel. yield in  
344 figure 12, supplement). This disagreement should not be an experimental artefact, again due  
345 to the high projectile current. The initial BeO layer on the sample formed in atmosphere  
346 (figure 9) is later removed in the experiment (figure 14, supplement). This is similar to the in  
347 situ sputter cleaning, but on a much longer timescale than for hydrocarbon impurities (days  
348 compared to minutes). Another possible artefact would be creating BeO from surface water,  
349 but when  $BeO^+$  and  $BeOH^+$  yields are compared in any figure, one sees that their behavior for  
350 various temperatures is very different. The  $BeO^+$  yield even decreases by higher  $H_2O$  partial  
351 pressures (in the relevant regime, figure 8), as discussed in the next section.

352 The  $BeD^+$  temperature dependent yield follows the  $Be^+$  trend, with the relative yield  
353  $BeD^+/Be^+$  falling linearly from 0.108(8) at room temperature to 0.032(1) at 723 K (figure 5  
354 and figure 12, supplement). The influence of the 540 K  $BeD_2$  decomposition from  
355 temperature-programmed desorption (TPD) measurements [5] seems to be small, as well as  
356 the desorption of implanted D around 460 K [31], [32]. Still, both are possible explanations of  
357 the  $BeD^+$  yield not rising further in that range. As mentioned above, this decrease is  
358 consistently found throughout various experiments [27] and in theory [28], [30].

### 359 **5.2.3 Projectile current scan**

360 The surface current was scanned, in order to see ion-flux dependencies. The beam diameter  
361 varies with projectile energy and cannot be measured in situ. An ex situ estimate (figure 14)  
362 suggests at least  $10^{17}$  ions  $m^{-2} s^{-1}$  for 20 nA surface current, likely more.





363  
364

365 *6: Relative yield for BeH<sup>+</sup> and BeD<sup>+</sup> depending on the surface current. The BeD<sup>+</sup> value at 24*  
 366 *nA is considered an artefact, caused by the process not being in equilibrium in that particular*  
 367 *mass spectrum. The absolute Be<sup>+</sup> yield (figure 13, supplement) and interestingly also BeD<sup>+</sup>*  
 368 *increase linearly with surface current, indicating a direct, one-particle process. Exponential*  
 369 *behavior of BeH<sup>+</sup> agrees with sputter cleaning. D<sub>2</sub><sup>+</sup> impacting Be at 673 K with 90 eV.*

370 The absolute Be<sup>+</sup> yield (figure 13, supplement) increases linearly with the surface current, as  
 371 expected for a direct knockout. A linear fit of ion yield [counts extraction<sup>-1</sup>] =  $s \times$   
 372  $I_{surf}$  [nA], results in a slope  $s = 7.3 (1)$  [counts extraction<sup>-1</sup> nA<sup>-1</sup>] for the Be<sup>+</sup> yield. For  
 373 BeD<sup>+</sup> a quadratic behavior is anticipated, for an expected two-step, e.g. a two-particle process:  
 374 The first D<sub>2</sub><sup>+</sup> projectile forms a BeD (or BeD<sub>2</sub>) on the surface, and then the second projectile  
 375 sputters it away as BeD<sup>+</sup>.

376 However, we find a clearly linear behavior. Thus, it is either a one-particle process as well, or  
 377 more likely one of the steps involved strongly assisted by the beryllium surface. A surprising  
 378 result, as it points towards a direct process, or a quasi-direct process at least.

379 The linear rise with no measured onset of saturation also implies a high relevance of the  
 380 projectile reaction channel when the flux is scaled from an ion beam experiment to a tokamak.  
 381 The BeD<sup>+</sup> absolute yield increases over flux with a slope of  $s =$   
 382  $2.53 (2)$  [counts extraction<sup>-1</sup> nA<sup>-1</sup>], which shows as a constant relative yield in figure 6.

383 There was a certain concern that the BeD<sup>+</sup> may have been formed from the D<sub>2</sub> gas leaking  
 384 from the ion source through the gas barrier into the vacuum chamber of the surface. In the  
 385 supplementary material, there are two measurements reported, which clearly show that the

386 small amounts of neutral  $D_2$  in the surface chamber do not play a role in the measurements  
 387 above. For very high  $D_2$  partial pressures, it is possible to form  $BeD^+$  from adsorbates as well,  
 388 analogous to the next section.

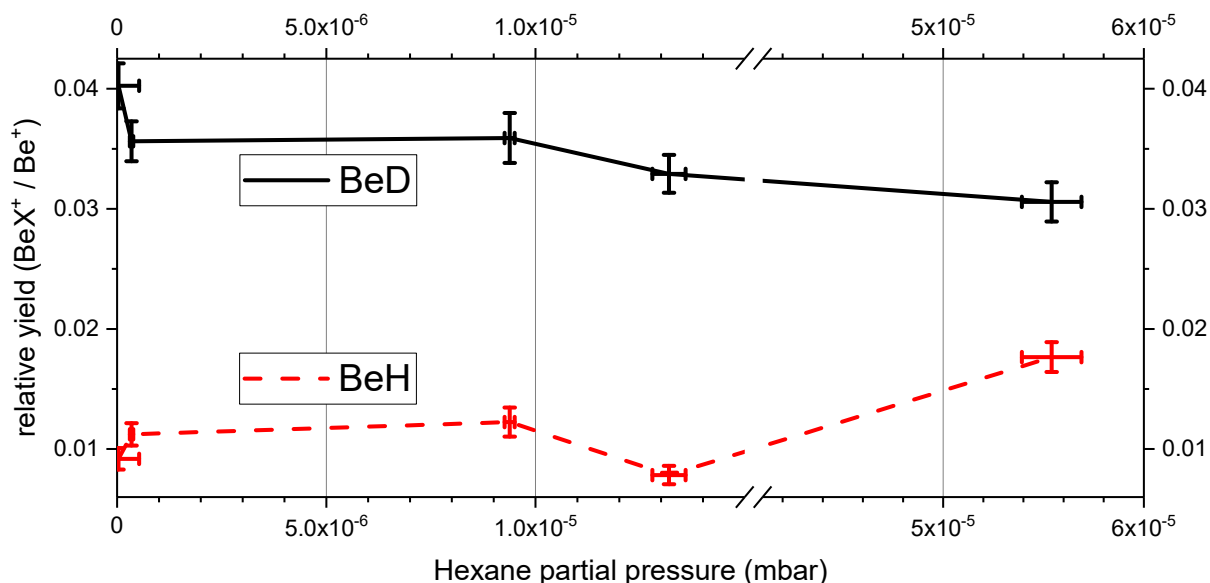
### 389 **5.3 Formation of $BeH^+$ : the surface adsorbate channel**

390 This channel has only minor relevance to fusion reactors allover, but it will occur in the  
 391 context of cooling water impurities. However, it is important for ion beam experiments. The  
 392 information helps to understand impurities in ion beam experiments and demonstrate, that  
 393 they do not influence the projectile reaction (yielding  $BeD^+$ ), if sufficiently high surface  
 394 currents and temperatures are used.

395 Indeed, the beryllium hydride synthesis was discovered in our experiment via impurities.  
 396  $BeH^+$  was produced, when a Be surface was bombarded with  $Ar^+$  ions (inset in figure 2):  
 397 Without intentionally providing hydrogen, a very low reactant concentration in other words,  
 398  $BeH^+$  is produced. This points towards an efficient mechanism producing a stable species.  
 399 Consistent with the sputter cleaning, high currents lead to a lower relative  $BeH^+$  yield (figure  
 400 6). Therefore, possible impurity candidates are tested by introducing them into the surface  
 401 collision chamber and varying their partial pressure.

#### 402 **5.3.1 $C_6H_{14}$ pressure scan**

403 First, to serve as a model system for long hydrocarbons, hexane ( $C_6H_{14}$ ) vapor was introduced  
 404 into the surface chamber (figure 7). Hydrocarbons from diffused pump oils were so far the  
 405 dominant impurity in similar setups.



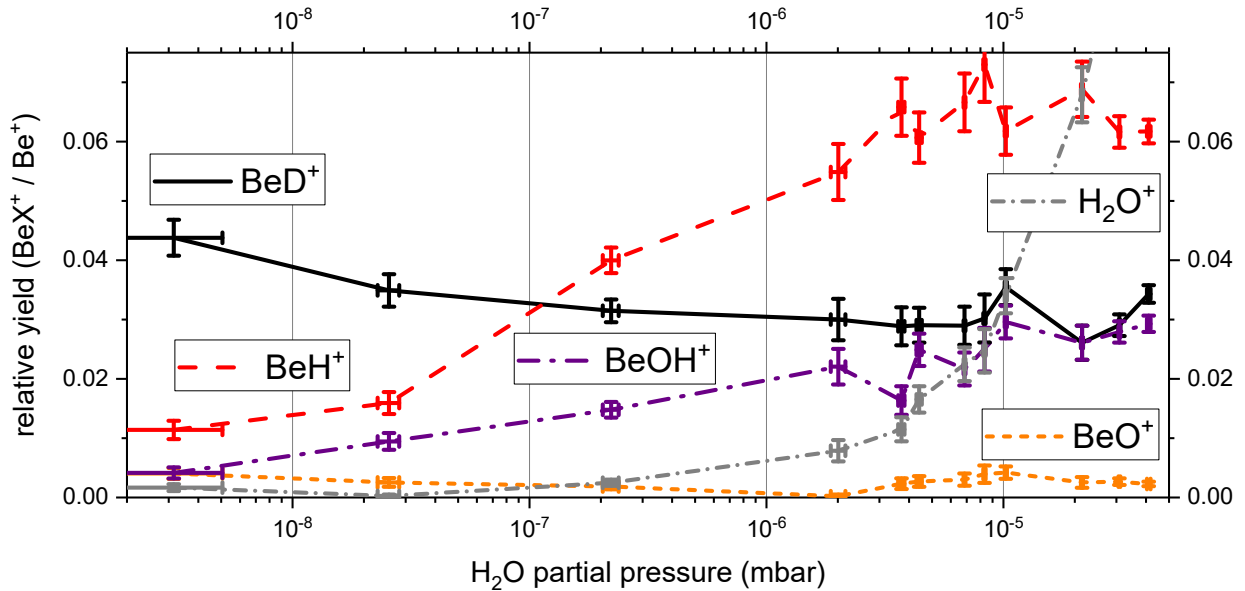
406  
 407

408 *7: Relative yield with different hexane partial pressures. Hexane adsorbate is not a good*  
 409 *source for hydrogen in BeH<sup>+</sup>. D<sub>2</sub><sup>+</sup> projectiles impacting Be at 673 K with 90 eV and*  
 410 *16.0(2) nA. D<sub>2</sub> partial pressure 1.0(1) × 10<sup>-6</sup> mbar.*

411 It increases the BeH<sup>+</sup> yield only by a factor of about two, when the hexane partial pressure is  
 412 above 5.5 × 10<sup>-5</sup> mbar. That is at least a factor 4000 more than the absolute residual gas  
 413 pressure. This excludes hydrocarbons as a possible hydrogen source. Hexane also suppresses  
 414 the BeD<sup>+</sup> production slightly, it likely starts to form a layer on top of the metal.

### 415 5.3.2 H<sub>2</sub>O pressure scan

416 Water vapor, the natural residual gas component, was tested next:



417  
418

419 *8: Relative yield using different H<sub>2</sub>O partial pressures. Strong BeH<sup>+</sup> synthesis already with*  
 420 *little H<sub>2</sub>O adsorption. D<sub>2</sub><sup>+</sup> projectiles impacting Be at 673 K with 90 eV and 16.1(4) nA. D<sub>2</sub>*  
 421 *partial pressure 1.0(1) × 10<sup>-6</sup> mbar.*

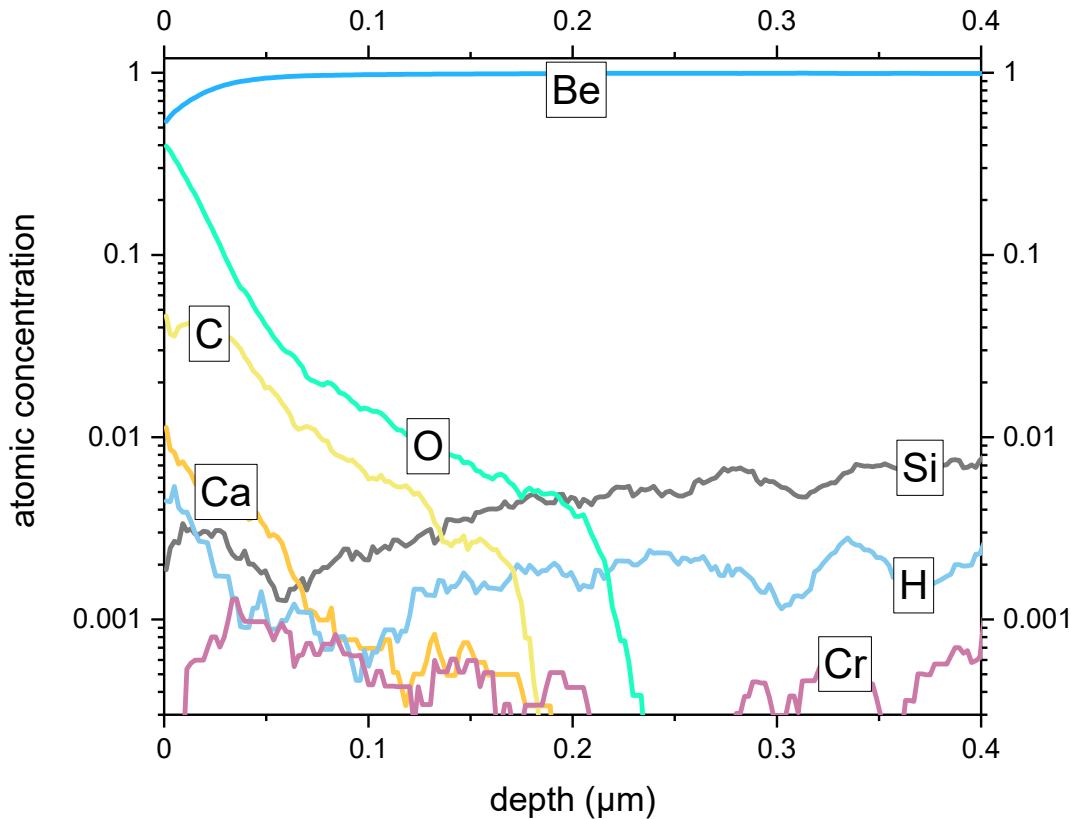
422 Already small amounts of water vapor in the surface chamber (figure 8) lead to a sharp  
 423 increase in the BeH<sup>+</sup> yield, which even crosses the BeD<sup>+</sup> yield at about 3 × 10<sup>-7</sup> mbar. The  
 424 attenuation of the BeD<sup>+</sup> production by the water being present is also more pronounced than  
 425 with hexane, which points towards longer sticking time due to its polar nature.

426 The less abundant BeOH<sup>+</sup> product shows the same energy and temperature behavior as BeH<sup>+</sup>,  
 427 indicating the formation from absorbed water.

## 428 5.4 TOF-ERDA: elemental composition profile

429 This section shows that a possible third channel for beryllium hydride synthesis connected  
 430 with the bulk hydrogen in the beryllium sample only plays a minor role. Therefore, an  
 431 elemental composition profile was recorded using TOF-ERDA in Uppsala ([33], results figure  
 432 9), after the surface was used in the SurfTOF experiment.

433



434

435 *9: TOF-ERDA [33] elemental profile analysis: Atom number concentration, 15 points*  
 436 *adjacent average smoothing,  $I^{8+}$  projectiles with 36 MeV. Consistent with SurfTOF data. On*  
 437 *the surface: Oxides attributed to the transport in air, C and H result from hydrocarbon*  
 438 *impurities. In the bulk, Si, H and Cr are remnants of the production process.*

439 The hydrogen number concentration in the bulk material is around 0.002 (figure 9). In order  
 440 to clarify ratios: Assuming exactly  $\frac{2H}{1000 Be} = 0.002$ , the maximum BeH/Be yield to be obtained  
 441 is  $\frac{2 BeH}{998 Be} \approx 0.002004$ , if all hydrogen is sputtered as BeH. The ionized ratio may still be  
 442 different, but for a basic investigation, the H/Be ratio serves as an upper boundary for  
 443  $BeH^+/Be^+$  obtained from the bulk.

444 However, we consistently measure a  $BeH^+/Be^+$  ratio of 0.008 at a given surface current and  
 445 temperature (figure 4, 6, 10, and 11). This confirms, that the bulk hydrogen can only be a

446 small source for hydrogen in  $\text{BeH}^+$ . Nevertheless, one can estimate the bulk hydrogen  
 447 contribution also from the SurfTOF data alone. As sputter cleaning is a rate model, the  
 448  $\text{BeH}^+/\text{Be}^+$  ratio ( $Y$ ) will follow an exponential behavior with the surface current:

$$449 \quad Y = A e^{\frac{-I_{\text{Surf}}}{t}} + y_0$$

450 The exponential part contains the idea of sputter cleaning a surface adsorbate.  $A$  is the  
 451 amplitude specific for  $\text{BeH}^+$  products,  $t$  describes how sensitive they are to differences in ion  
 452 current. It contains the assumption  $I_{\text{Surf}} \gg 0$ , meaning there is sufficient projectile flux,  
 453 removing all hydrogen that is adsorbed. The constant term,  $y_0$ , is the underlying contribution  
 454 from bulk hydrogen. It has to be current-independent.

455 We obtain  $y_0 = 0.0043(6)$  by a fit to the current scan (figure 6). As this is still about twice the  
 456  $\text{H}/\text{Be} = 0.002$ , we conclude:

- 457 • There is only a minor contribution from bulk hydrogen to the overall  $\text{BeH}^+/\text{Be}^+$  ratio.
- 458 • The exponential curve fits the data very well, proving sputter cleaning as a valid  
 459 concept.
- 460 • The largest uncertainty remaining is the ion-to-neutral ratio, which we will address in  
 461 future experiments.

462 The hydrogen impurities come from the industrial production process in a hydrogen  
 463 atmosphere. Together with Si from the ore and Cr they are the only impurities contained in  
 464 the bulk material.

465 On top of the surface, there is a thick oxide layer found (more than 1 % O along the top 0.1  
 466  $\mu\text{m}$ ). It mostly originates from the sample being transferred in atmosphere for a couple of  
 467 days between the experiments. But even this thick oxide layer is removed in the SurfTOF  
 468 experiment in the timespan of a few weeks. Creating an optical 3D model of the surface  
 469 before and after bombardment of the surface, we estimate that 1.0(5)  $\mu\text{m}$  of material was  
 470 removed perpendicular to the surface, with a FWHM beam cross section of about 1.5  $\text{mm}^2$  in  
 471 about 4 months. (figure 14, supplement, using an “infinite focus microscope” [34]).

472 This also gives information about the much thinner oxygen layer, that could form from  
 473 residual gas in the UHV apparatus. During measurements, it cannot be formed, as the ion flux  
 474 is at least in the same order of magnitude than the neutral gas flux to the surface. If it formed  
 475 between the measurements, beryllium oxide yields would decrease during long  
 476 measurements, which they do not. This means, in total, in-situ sample oxidation is very little.

477 The reason for calcium found on the surface in low concentration remains unclear, but it is  
478 seen in the mass spectra from SurfTOF as well, mainly due to its high ionization probability.

479 There was no implantation of deuterium observed, consistent with experiments and MD  
480 simulations at elevated temperatures [5], [31], [32], [35]. This supports the idea, that  $\text{BeD}^+$  is  
481 formed in a (quasi-)direct reaction with the projectile and not from implantation.

## 482 **6 Conclusion and outlook**

483 A new type of research apparatus was built that enables efficient in situ sputter cleaning by a  
484 very high projectile current. This also allows to reach equilibrium conditions for all processes  
485 described here. Both are responsible for outstanding data quality and repeatability. The unique  
486 measurements describe chemical sputtering in detail, down to a molecular picture.

487 The beryllium surface plays a much bigger role than only providing the reactant for the  
488 beryllium hydride formation: In the synthesis from the impacting ion, it assists the presumed  
489 multi-step reaction, leading to a direct process (linear surface flux dependency). Its many  
490 degrees of freedom also take away excess energy in a reaction, as it is still possible to form  
491  $\text{BeD}^+$  at an impact energy of 426 eV. We observe that all hydride products do not require  
492 more energy to form than is needed to sputter them towards the detector. In fact, the  
493 maximum relative yield of  $\text{BeD}^+/\text{Be}^+$  of 2.75 is reached at 20 eV, the lowest impact energy  
494 measured.

495 Comparing the  $\text{BeD}^+$  yield to findings from experimental fusion reactors, the qualitative  
496 image fits very well. Its quantitative relevance should be further clarified using tailored  
497 simulations. Also the higher fluxes in a tokamak device will impact the  $\text{BeD}^+/\text{Be}^+$  ratio  
498 obtained. However, flux dependencies measured in this work point towards an effective  
499 mechanism also at higher fluxes. Allover it offers substantial evidence for molecular tritium  
500 retention in beryllium co-deposits, which we did not find discussed in the literature. It is an  
501 alarming fact, that we could produce at least some  $\text{BeD}^+$  using any projectile energy and  
502 surface temperature accessible.

503 The second reaction channel, forming beryllium hydrides from surface adsorbates was clearly  
504 identified. The product ion yield does not depend on projectile properties (species, kinetic  
505 energy), but on the surface condition (temperature, surface ion flux).

506 Surface adsorbates will not play a decisive role for thermonuclear fusion, nevertheless we  
 507 showed that adsorbate surface chemistry is still efficient at high temperatures. Even at 723 K,  
 508 molecules remain on the surface for a long enough time to react with impacting ions. This  
 509 should be kept in mind, as fusion devices deal with seeding gases and impurities, especially  
 510 cooling water.

511 Experimental concerns were carefully ruled out, discovering a possible third reaction channel.  
 512  $\text{BeH}^+$  might also be formed from impurities in the bulk, similar to the adsorbate mechanism.

513 In general, beryllium is not as reactive as the previously used carbon (CFC), but metal  
 514 surfaces bombarded with ions pose ideal conditions for a rich chemistry. In future, neutral  
 515 products, as well as  $\text{D}^+$  and  $\text{N}^+$  projectiles will be examined. The latter is motivated by the fact  
 516 of nitrogen seeding causing more tritium retention [36], pointing towards chemistry as well.  
 517 Also, reactions of high-Z materials, such as tungsten hydrides, are of interest for the proposed  
 518 all-tungsten design of a commercial reactor [37].

## 519 7 Acknowledgments

520 We kindly like to thank Daniel Primetzhofer, the Swedish Research Council and the Swedish  
 521 Foundation for Strategic Research for making the TOF-ERDA measurements possible. Our  
 522 work is supported by Friedrich Schiedel Foundation for Energy Technology 259564,  
 523 “Reaktive Ionen-Oberflächenstöße”. Austrian Science Fund (FWF) W1259-N27 „DK-ALM“.  
 524 This work has been carried out within the framework of the EUROfusion Consortium and has  
 525 received funding from the Euratom research and training programme 2014-2018 under grant  
 526 agreement No 633053. The views and opinions expressed herein do not necessarily reflect  
 527 those of the European Commission.

## 528 8 References

- 529 [1] X. Litaudon *et al.*, “Overview of the JET results in support to ITER,” *Nucl. Fusion*, vol.  
 530 57, no. 10, p. 102001, 2017.
- 531 [2] M. Shimada *et al.*, “In-vessel dust and tritium control strategy in ITER,” *J. Nucl. Mater.*,  
 532 vol. 438, Supplement, pp. S996–S1000, Jul. 2013.
- 533 [3] G. Federici *et al.*, “In-vessel tritium retention and removal in ITER,” *J. Nucl. Mater.*, vol.  
 534 266–269, pp. 14–29, Mar. 1999.

- 535 [4] G. De Temmerman *et al.*, “Efficiency of thermal outgassing for tritium retention  
536 measurement and removal in ITER,” *Nucl. Mater. Energy*, 2017.
- 537 [5] R. P. Doerner, M. J. Baldwin, D. Buchenauer, G. De Temmerman, and D. Nishijima,  
538 “The role of beryllium deuteride in plasma-beryllium interactions,” *J. Nucl. Mater.*, vol.  
539 390–391, pp. 681–684, Jun. 2009.
- 540 [6] Y. Hirooka *et al.*, “A new plasma-surface interactions research facility: PISCES-B and  
541 first materials erosion experiments on bulk-boronized graphite,” *J. Vac. Sci. Technol. Vac.*  
542 *Surf. Films*, vol. 8, no. 3, pp. 1790–1797, May 1990.
- 543 [7] D. Nishijima, R. P. Doerner, M. J. Baldwin, G. D. Temmerman, and E. M. Hollmann,  
544 “Properties of BeD molecules in edge plasma relevant conditions,” *Plasma Phys. Control.*  
545 *Fusion*, vol. 50, no. 12, p. 125007, 2008.
- 546 [8] G. Federici *et al.*, “Plasma-material interactions in current tokamaks and their  
547 implications for next step fusion reactors,” *Nucl. Fusion*, vol. 41, no. 12, p. 1967, 2001.
- 548 [9] P. C. Smith and D. N. Ruzic, “Low energy (10 to 700 eV) angularly resolved sputtering  
549 yields for D + on beryllium,” *Nucl. Fusion*, vol. 38, no. 5, p. 673, 1998.
- 550 [10] J. Bohdanský and J. Roth, “Light ion sputtering of low Z materials in the temperature  
551 range 20–1100°C,” *J. Nucl. Mater.*, vol. 123, no. 1, pp. 1417–1424, May 1984.
- 552 [11] J. Roth, J. Bohdanský, R. S. Blewer, W. Ottenberger, and J. Borders, “Sputtering of  
553 Be and BeO by light ions,” *J. Nucl. Mater.*, vol. 85–86, pp. 1077–1079, Dec. 1979.
- 554 [12] A. Keim, M. Harnisch, P. Scheier, and Z. Herman, “Collisions of low-energy ions Ar<sup>+</sup>  
555 and N<sub>2</sub><sup>+</sup> with room-temperature and heated surfaces of tungsten, beryllium, and a mixed  
556 beryllium–tungsten thin film,” *Int. J. Mass Spectrom.*, vol. 354–355, pp. 78–86, Nov.  
557 2013.
- 558 [13] M. Harnisch, A. Keim, P. Scheier, and Z. Herman, “Formation of HCN<sup>+</sup> in  
559 Heterogeneous Reactions of N<sub>2</sub><sup>+</sup> and N<sup>+</sup> with Surface Hydrocarbons,” *J. Phys. Chem. A*,  
560 vol. 117, no. 39, pp. 9653–9660, Oct. 2013.
- 561 [14] M. Harnisch, A. Keim, P. Scheier, and Z. Herman, “Collisions of low-energy Ar<sup>+</sup>,  
562 N<sub>2</sub><sup>+</sup>, and D<sub>2</sub><sup>+</sup> ions with room-temperature and heated surfaces of mixed beryllium–  
563 tungsten thin films of different composition,” *Int. J. Mass Spectrom.*, vol. 365–366, pp.  
564 316–323, May 2014.
- 565 [15] V. Grill, R. Wörgötter, J. H. Futrell, and T. D. Märk, “Surface induced reactions of  
566 cluster ions,” *Z. Für Phys. AtomsMolecules Clust.*, vol. 40, no. 1, pp. 111–114, Mar. 1997.
- 567 [16] J. Žabka, Z. Dolejšek, J. Roithová, V. Grill, T. D. Märk, and Z. Herman, “Energy  
568 partitioning in collisions of slow polyatomic ions with carbon surfaces,” *Int. J. Mass*  
569 *Spectrom.*, vol. 213, no. 2, pp. 145–156, Feb. 2002.
- 570 [17] M. A. Mabud, M. J. Dekrey, and R. Graham Cooks, “Surface-induced dissociation of  
571 molecular ions,” *Int. J. Mass Spectrom. Ion Process.*, vol. 67, no. 3, pp. 285–294, Nov.  
572 1985.
- 573 [18] V. H. Wysocki, J.-M. Ding, J. L. Jones, J. H. Callahan, and F. L. King, “Surface-  
574 induced dissociation in tandem quadrupole mass spectrometers: A comparison of three  
575 designs,” *J. Am. Soc. Mass Spectrom.*, vol. 3, no. 1, pp. 27–32, Jan. 1992.
- 576 [19] E. N. Rudisill, J. J. Hacskeylo, and M. D. LeVan, “Coadsorption of hydrocarbons and  
577 water on BPL activated carbon,” *Ind. Eng. Chem. Res.*, vol. 31, no. 4, pp. 1122–1130,  
578 Apr. 1992.



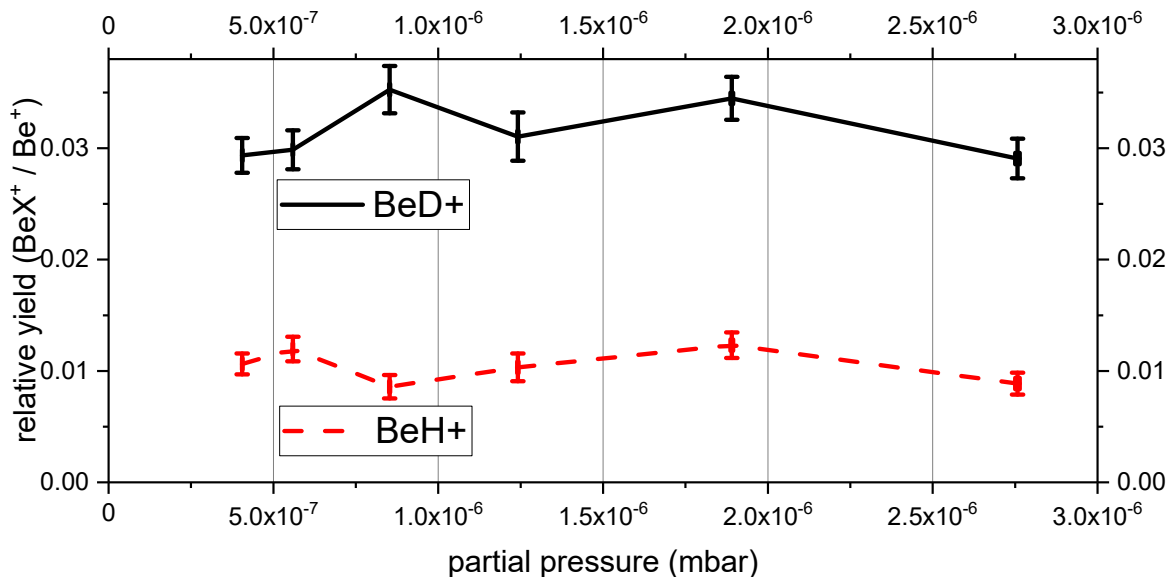
- 579 [20] R. J. Pearce *et al.*, “The ITER divertor pumping system, design evolution,  
580 simplification and performance,” *Fusion Eng. Des.*, vol. 88, no. 6, pp. 809–813, Oct.  
581 2013.
- 582 [21] R. A. Pitts *et al.*, “Status and physics basis of the ITER divertor,” *Phys. Scr.*, vol.  
583 2009, no. T138, p. 014001, 2009.
- 584 [22] J. H. Leck, *Total and Partial Pressure Measurement in Vacuum Systems*. Springer US,  
585 1989.
- 586 [23] B. Wolf, *Handbook of Ion Sources*. CRC Press, 1995.
- 587 [24] M. Harnisch, P. Scheier, and Z. Herman, “Heterogeneous reactions between ions  
588 NH<sub>3</sub><sup>+</sup> and NH<sup>+</sup> and hydrocarbons adsorbed on a tungsten surface. Formation of HCN<sup>+</sup> in  
589 NH<sup>+</sup>-surface hydrocarbon collisions,” *Int. J. Mass Spectrom.*, vol. 392, pp. 139–144, Dec.  
590 2015.
- 591 [25] J. Kubišta, Z. Dolejšek, and Z. Herman, “Energy Partitioning in Collisions of Slow  
592 Polyatomic Ions with Surfaces: Ethanol Molecular Ions on Stainless Steel Surfaces,” *Eur.*  
593 *Mass Spectrom.*, vol. 4, no. 5, pp. 311–319, Oct. 1998.
- 594 [26] M. Harnisch, “Ion-surface collisions of slow ions with fusion-relevant surfaces,” Phd,  
595 University of Innsbruck, 2015.
- 596 [27] S. Brezinsek *et al.*, “Study of physical and chemical assisted physical sputtering of  
597 beryllium in the JET ITER-like wall,” *Nucl. Fusion*, vol. 54, no. 10, p. 103001, 2014.
- 598 [28] I. Sukuba, A. Kaiser, S. E. Huber, J. Urban, and M. Probst, “Energetics and reactivity  
599 of small beryllium deuterides,” *J. Mol. Model.*, vol. 23, no. 7, p. 203, Jul. 2017.
- 600 [29] R. P. Doerner *et al.*, “Codeposition of deuterium with ITER materials,” *Nucl. Fusion*,  
601 vol. 49, no. 3, p. 035002, 2009.
- 602 [30] E. Safi, G. Valles, A. Lasa, and K. Nordlund, “Multi-scale modelling to relate  
603 beryllium surface temperature, deuterium concentration and erosion in fusion reactor  
604 environment,” *J. Phys. Appl. Phys.*, vol. 50, no. 20, p. 204003, 2017.
- 605 [31] M. Oberkofler, M. Reinelt, A. Allouche, S. Lindig, and C. Linsmeier, “Towards a  
606 detailed understanding of the mechanisms of hydrogen retention in beryllium,” *Phys. Scr.*,  
607 vol. 2009, no. T138, p. 014036, 2009.
- 608 [32] M. Oberkofler and C. Linsmeier, “Deuterium release from implanted beryllium and  
609 beryllium oxide,” *J. Nucl. Mater.*, vol. 415, no. 1, Supplement, pp. S724–S727, Aug.  
610 2011.
- 611 [33] Y. Zhang *et al.*, “Detection efficiency of time-of-flight energy elastic recoil detection  
612 analysis systems,” *Nucl. Instrum. Methods Phys. Res. Sect. B Beam Interact. Mater. At.*,  
613 vol. 149, no. 4, pp. 477–489, Mar. 1999.
- 614 [34] “InfiniteFocus,” *Alicona – That’s metrology*, 09-Feb-2018. [Online]. Available:  
615 <http://www.alicon.com/products/infinitefocus/>. [Accessed: 23-Apr-2018].
- 616 [35] E. Safi, C. Björkas, A. Lasa, K. Nordlund, I. Sukuba, and M. Probst, “Atomistic  
617 simulations of the effect of reactor-relevant parameters on be sputtering,” *J. Nucl. Mater.*,  
618 vol. 463, pp. 805–809, Aug. 2015.
- 619 [36] M. Oberkofler *et al.*, “First nitrogen-seeding experiments in JET with the ITER-like  
620 Wall,” *J. Nucl. Mater.*, vol. 438, pp. S258–S261, Jul. 2013.
- 621 [37] G. Janeschitz, “Plasma–wall interaction issues in ITER,” *J. Nucl. Mater.*, vol. 290–  
622 293, pp. 1–11, Mar. 2001.

623

## 624 9 Supplementary material

### 625 9.1.1 D<sub>2</sub> pressure scan, D<sub>2</sub><sup>+</sup> projectile

626 There was a certain concern that the BeD<sup>+</sup> may have been formed from the D<sub>2</sub> gas leaking  
 627 from the ion source through the gas barrier into the vacuum chamber of the surface. Though  
 628 the low sticking probability of D<sub>2</sub> (a non-polar, light molecule) on a 673 K surface contradicts  
 629 this idea already, as well as the surface current scan does (figure 6), we ran experiments  
 630 showing that this is not the case.

631  
632

633 *10: The relative BeD<sup>+</sup> yield does not depend on the D<sub>2</sub> partial pressure in the surface*  
 634 *chamber. D<sub>2</sub><sup>+</sup> projectiles impacting Be at 673 K with 90 eV and 5.6(2) nA.*

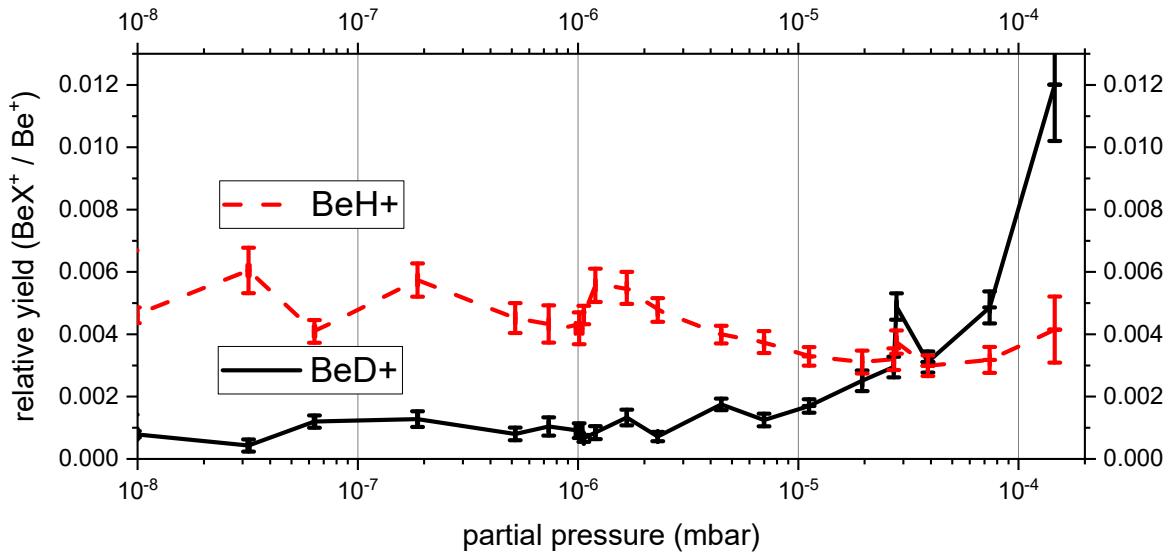
635 By changing the D<sub>2</sub> pressure in the quadrupole chamber and adjusting the ion source, a  
 636 constant surface current of 5.6(2) nA was achieved at different D<sub>2</sub> partial pressures in the  
 637 surface chamber. This is about 4 times lower current than in the other measurements reported  
 638 here, but it should increase the relative yields from surface adsorbates (inverse sputter  
 639 cleaning). As can be seen in figure 10, neither BeD<sup>+</sup> nor BeH<sup>+</sup> depend on the neutral D<sub>2</sub>  
 640 partial pressure.

641 This already shows that the neutral D<sub>2</sub> does not influence the measurements in the relevant  
 642 regime, but to be sure we are not measuring a saturated adsorption process, an exchange of  
 643 the projectile to He<sup>+</sup> allows to remove any neutral D<sub>2</sub> from the surface chamber.

644

645 **9.1.2 D<sub>2</sub> pressure scan, He<sup>+</sup> projectile**

646 The following graph was obtained using He<sup>+</sup> projectiles and different D<sub>2</sub> partial pressures in the surface chamber. While the BeH<sup>+</sup> relative yield remains unchanged, BeD<sup>+</sup> is far below its  
 647 usual level and increases only at very high partial pressures.  
 648



649

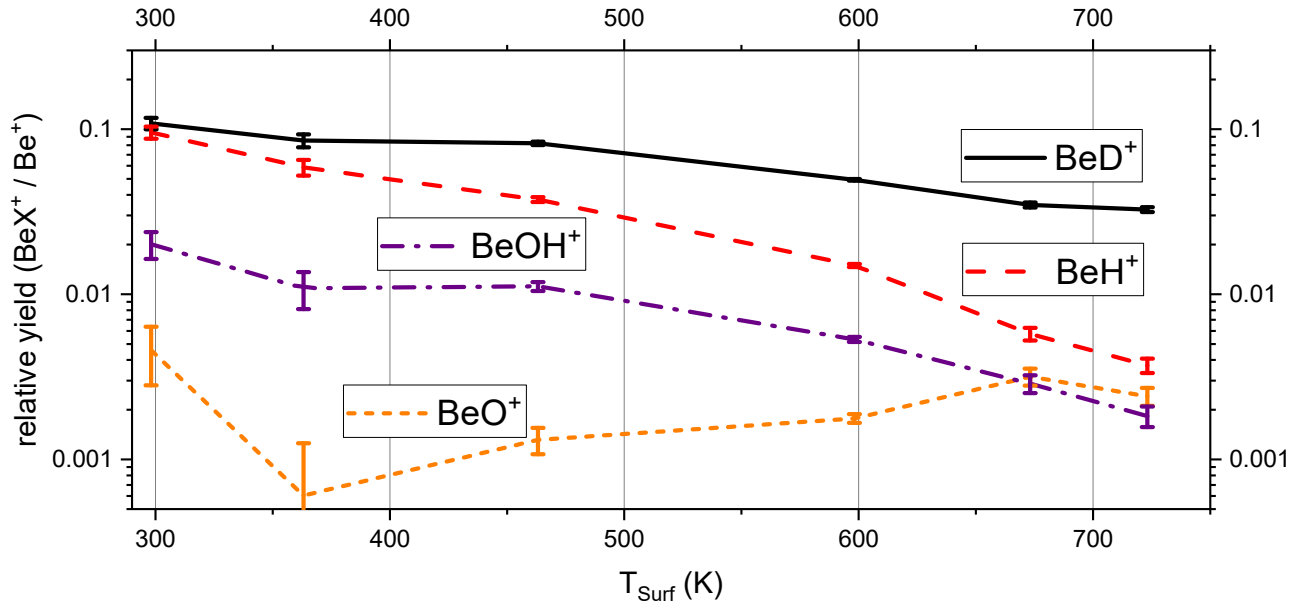
650 *11: He<sup>+</sup> projectiles impacting Be at 673 K with 90 eV and 5.7(2) nA. Relative yield with*  
 651 *different D<sub>2</sub> partial pressures in the surface chamber. BeH<sup>+</sup> yield remains unchanged, albeit*  
 652 *the different projectile. BeD<sup>+</sup> forms from adsorbates only at very high partial pressures. He*  
 653 *partial pressure 1.1(2) × 10<sup>-7</sup> mbar.*

654 Despite He<sup>+</sup> and D<sub>2</sub><sup>+</sup> having the same nominal mass, exchanging the projectile should alter the  
 655 sputter yields as they are products of a chemical reaction. This indeed is the case when the  
 656 projectile reacts; but for the surface adsorbate channel, the projectile seems to provide the  
 657 activation energy only. This can easily be seen, as the BeH<sup>+</sup>/Be<sup>+</sup> ratio is constant (around  
 658 0.008 at 673 K, compare figure 4, 6, and 10 with figure 11), and is very close to this value  
 659 when the projectile is changed from D<sub>2</sub><sup>+</sup> to He<sup>+</sup>. As BeH<sup>+</sup> and BeD<sup>+</sup> are chemically identical,  
 660 the BeD<sup>+</sup> relative yield would not depend on the type of projectile, if BeD<sup>+</sup> was formed from  
 661 surface adsorbates as well. Instead, it drops by a factor of 30 down to the background level (at  
 662 relevant D<sub>2</sub> pressure 1.0(1) × 10<sup>-6</sup> mbar, compare again figure 4, 6, and 10 with figure 11).  
 663 This confirms the D<sub>2</sub><sup>+</sup> projectile and clearly excludes the D<sub>2</sub> neutral adsorbate being  
 664 responsible for the BeD<sup>+</sup> production.

665 Additionally, figure 11 shows the onset of the surface adsorbate channel, which also exists for  
 666 BeD<sup>+</sup>, but only for D<sub>2</sub> partial pressures of much more than 10<sup>-5</sup> mbar – D<sub>2</sub> adsorption to the

667 surface is irrelevant for the SurfTOF experiment, but might be a concern in fusion devices in  
 668 regions of high neutral density, for example the divertor [8].

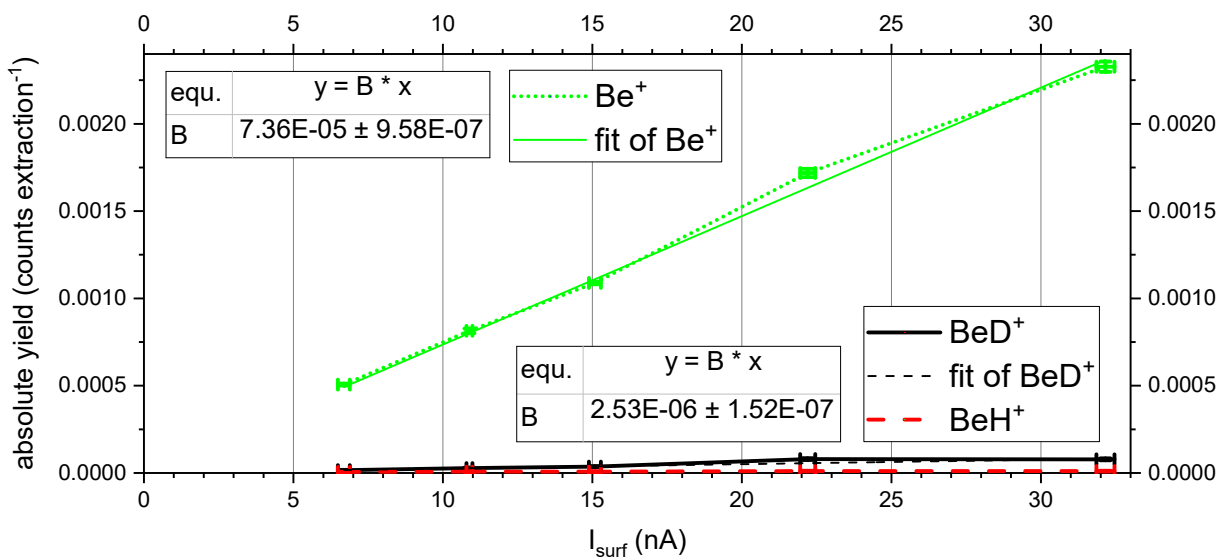
669 **9.2 Temperature scan, relative yield**



670  
 671

672 *12: Temperature dependence of the relative yield. The linear decrease of the  $\text{BeD}^+/\text{Be}^+$  ratio*  
 673 *( $\text{BeD}/\text{Be}$  respectively) with increasing  $T_{\text{Surf}}$  is found throughout different experiments [27],*  
 674 *theory and MD simulations [28], [30].  $\text{D}_2^+$  impacting Be with 90 eV and 16.1(2) nA.*

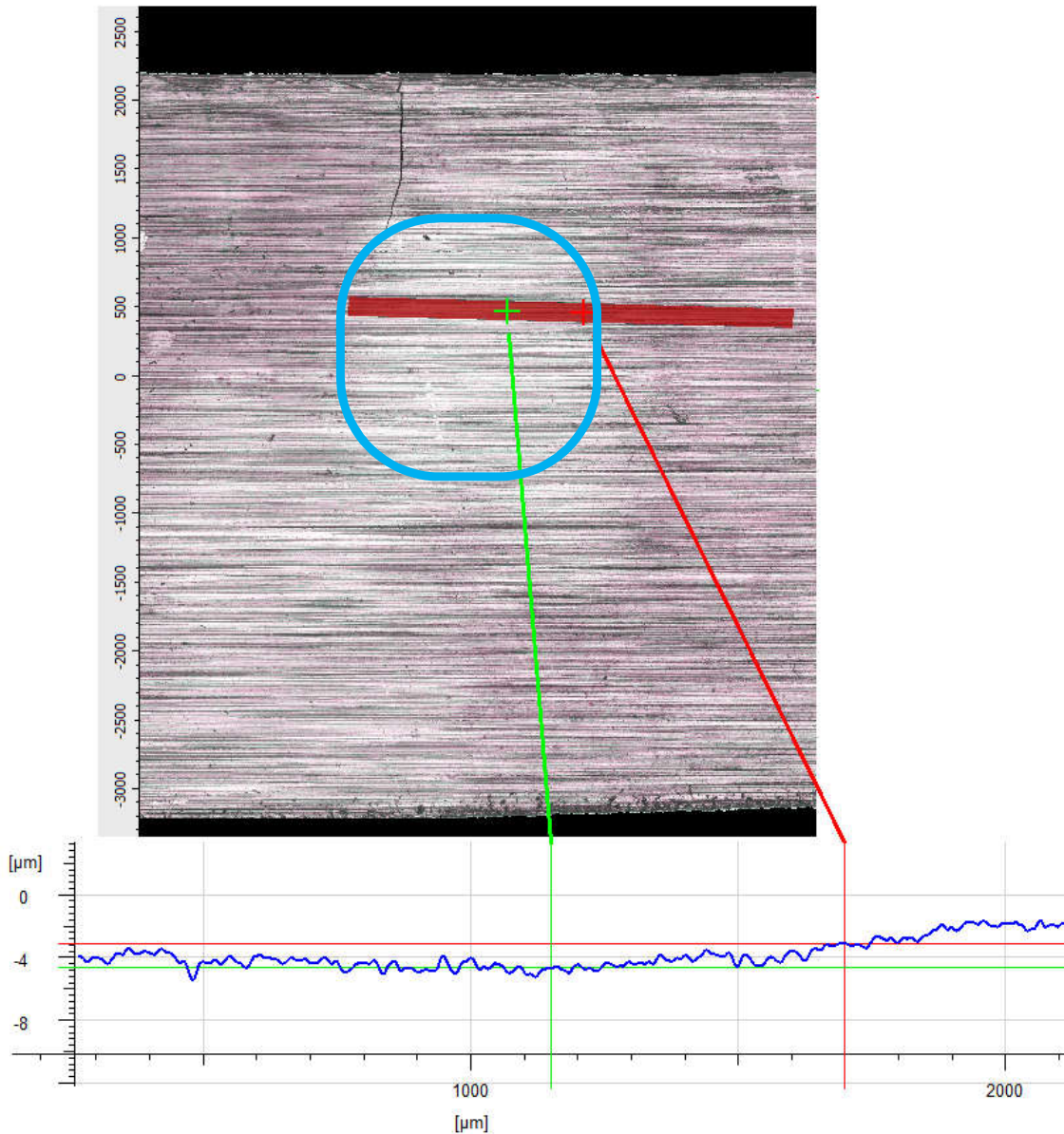
675 **9.3 Current scan, absolute yield**



676  
 677

678 *13: Absolute yield depending on the Surface current.  $\text{Be}^+$  and  $\text{BeD}^+$  yields are linear through*  
 679 *the origin, which identifies both as direct or a quasi-direct process.  $\text{BeH}^+$  behaves differently*  
 680 *(also figure 6) identifying the Surface adsorbate channel.  $\text{D}_2^+$  impacting Be with 90 eV,  $T_{\text{Surf}}$*   
 681 *is 673 K.*

## 682 9.4 3D surface profile



683

684

685 *14: Optical 3D profile scan of the rolled beryllium sample obtained using an Alicona IFM*  
 686 *[34]. The area marked in light blue (XY-plane) has been hit by the projectile, resulting in a*  
 687 *clearly different color of the beryllium. The Z-profile at the bottom shows, that this area has*  
 688 *lost approximately 1,0(5)  $\mu\text{m}$  of material (compare green and red cross).*